Article

Structural Chemistry of "Defect" Cyanometalate Boxes: {Cs⊂[CpCo(CN)][Cp*Ru]} and {M⊂[Cp*Rh(CN)][Cp*Ru]} (M = NH, Cs)

Matthew L. Kuhlman, and Thomas B. Rauchfuss

J. Am. Chem. Soc., **2003**, 125 (33), 10084-10092• DOI: 10.1021/ja035253h • Publication Date (Web): 26 July 2003

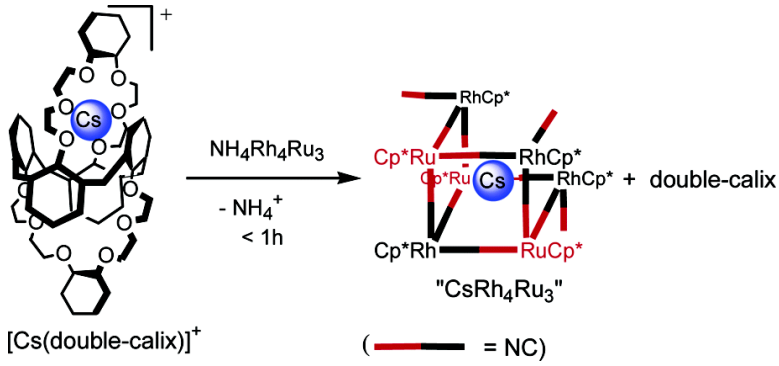

More About This Article

Additional resources and features associated with this article are available within the HTML version:

- Supporting Information
- Links to the 4 articles that cite this article, as of the time of this article download
- Access to high resolution figures
- Links to articles and content related to this article
- Copyright permission to reproduce figures and/or text from this article

View the Full Text HTML

J|A|C|S
ARTICLES
Published on Web 07/26/2003

Structural Chemistry of "Defect" Cyanometalate Boxes: {Cs⊂[CpCo(CN)$_3$]$_4$[Cp*Ru]$_3$} and {M⊂[Cp*Rh(CN)$_3$]$_4$[Cp*Ru]$_3$} (M = NH$_4$, Cs)

Matthew L. Kuhlman and Thomas B. Rauchfuss*

Contribution from the Department of Chemistry, University of Illinois at Urbana-Champaign, Urbana, Illinois 61801

Received March 20, 2003; E-mail: rauchfuz@uiuc.edu

Abstract: A series of heptametallic cyanide cages are described; they represent soluble analogues of defect-containing cyanometalate solid-state polymers. Reaction of 0.75 equiv of [Cp*Ru(NCMe)$_3$]PF$_6$, Et$_4$N-[Cp*Rh(CN)$_3$], and 0.25 equiv of CsOTf in MeCN solution produced {Cs⊂[Cp*Rh(CN)$_3$]$_4$[Cp*Ru]$_3$} (**Cs⊂Rh$_4$Ru$_3$**). ^{1}H and ^{133}Cs NMR measurements show that **Cs⊂Rh$_4$Ru$_3$** exists as a single C_s isomer. In contrast, {Cs⊂[CpCo(CN)$_3$]$_4$[Cp*Ru]$_3$} (**Cs⊂Co$_4$Ru$_3$**), previously lacking crystallographic characterization, adopts both C_s isomers in solution. In situ ESI-MS studies on the synthesis of **Cs⊂Rh$_4$Ru$_3$** revealed two Cs-containing intermediates, **Cs⊂Rh$_2$Ru$_2$**$^+$ (1239 *m*/*z*) and **Cs⊂Rh$_3$Ru$_3$**$^+$ (1791 *m*/*z*), which underscore the participation of Cs$^+$ in the mechanism of cage formation. ^{133}Cs NMR shifts for the cages correlated with the number of CN groups bound to Cs$^+$: **Cs⊂Co$_4$Ru$_4$**$^+$ (δ 1 vs δ 34 for CsOTf), **Cs⊂Rh$_4$Ru$_3$** where Cs$^+$ is surrounded by ten CN ligands (δ 91), **Cs⊂Co$_4$Ru$_3$**, which consists of isomers with 11 and 10 π-bonded CNs (δ 42 and δ 89, respectively). Although {K⊂[Cp*Rh(CN)$_3$]$_4$[Cp*Ru]$_3$} could not be prepared, {NH$_4$⊂-[Cp*Rh(CN)$_3$]$_4$[Cp*Ru]$_3$} (**NH$_4$⊂Rh$_4$Ru$_3$**) forms readily by NH$_4$$^+$-template cage assembly. IR and NMR measurements indicate that NH$_4$$^+$ binding is weak and that the site symmetry is low. CsOTf quantitatively and rapidly converts **NH$_4$⊂Rh$_4$Ru$_3$** into **Cs⊂Rh$_4$Ru$_3$**, demonstrating the kinetic advantages of the M$_7$ cages as ion receptors. Crystallographic characterization of **CsCo$_4$Ru$_3$** revealed that it crystallizes in the C_s-(exo)$_1$(endo)$_2$ isomer. In addition to the nine μ-CN ligands, two CN$_t$ ligands are π-bonded to Cs$^+$. **M⊂Rh$_4$Ru$_3$** (M = NH$_4$, Cs) crystallizes as the second C_s isomer, that is, (exo)$_2$(endo)$_1$, wherein only one CN$_t$ ligand interacts with the included cation. The distorted framework of **NH$_4$⊂Rh$_4$Ru$_3$** reflects the smaller ionic radius of NH$_4$$^+$. The protons of NH$_4$$^+$ were located crystallographically, allowing precise determination of the novel NH$_4$···CN interaction. A competition experiment between calix[4]arene-bis(benzocrown-6) and **NH$_4$⊂Rh$_4$Ru$_3$** reveals **NH$_4$⊂Rh$_4$Ru$_3$** has a higher affinity for cesium.

Introduction

Molecular containers are of continuing interest for synthetic chemists due to their realized uses as catalysts,[1,2] sorters,[3] sensors,[4,5] and in cavity directed synthesis.[6,7] Most molecular containers are based on hydrocarbon frameworks.[8] An advantage of inorganic frameworks is their potential rigidity, which should impart size-based selectivity to these supermolecules.[9] It has, however, proven difficult to synthesize inorganic molecular cages that exhibit host−guest behavior. Our approach to inorganic cages entails the use of the rigid organometallic cyanides. Cyanometalate building blocks indeed give rise to diverse structures such as chains,[10,11] triangles,[12,13] squares,[14−16] hexagons,[17] boxes,[18,19] and extended solid frameworks[20] which have been discussed as sensors,[21] molecular magnets,[22,23] and sieves.[24]

Much work on cyanometalate-based cages is inspired by Prussian Blue (PB), the inorganic polymer Fe$_7$(CN)$_{18}$(H$_2$O)$_x$.[25] PB is prepared by the building block approach, the condensation of [Fe(CN)$_6$]$^{4-}$ and Fe(III) salts (eq 1).

$$3[Fe(CN)_6]^{4-} + 4Fe^{3+} \rightarrow Fe_7(CN)_{18}(H_2O)_x \qquad (\text{"PB"}) \quad (1)$$

PB consists of CN-interconnected octahedral Fe centers, the

(1) Kang, J.; Santamaria, J.; Hilmersson, G.; Rebek, J., Jr. *J. Am. Chem. Soc.* **1998**, *120*, 7389−7390.
(2) Ito, H.; Kusukawa, T.; Fujita, M. *Chem. Lett.* **2000**, 598−599.
(3) Atwood, J. L.; Koutsantonis, G. A.; Raston, C. L. *Nature* **1994**, *368*, 229−231.
(4) Lehaire, M.-L.; Scopelliti, R.; Piotrowski, H.; Severin, K. *Angew. Chem., Int. Ed.* **2002**, *41*, 1419−1422.
(5) Beer, P. D.; Szemes, F.; Balzani, V.; Sala, C. M.; Drew, M. G. B.; Dent, S. W.; Maestri, M. *J. Am. Chem. Soc.* **1997**, *119*, 11864−11875.
(6) Yoshizawa, M.; Takeyama, Y.; Kusukawa, T.; Fujita, M. *Angew. Chem., Int. Ed.* **2002**, *41*, 1347−1349.
(7) Yoshizawa, M.; Kusukawa, T.; Fujita, M.; Sakamoto, S.; Yamaguchi, K. *J. Am. Chem. Soc.* **2001**, *123*, 10454−10459.
(8) Lehn, J. M. *Supramolecular Chemistry: Concepts and Perspectives*; VCH: Weinhiem, 1995.
(9) Huang, S. P.; Kanatzidis, M. G. *Angew. Chem., Int. Ed. Engl.* **1992**, *31*, 787−789.
(10) Chiorboli, C.; Bignozzi, C. A.; Indelli, M. T.; Rampi, M. A.; Scandola, F. *Coord. Chem. Rev.* **1991**, *111*, 267−274.
(11) Scandola, F.; Argazzi, R.; Bignozzi, C. A.; Chiorboli, C.; Indelli, M. T.; Rampi, M. A. *Coord. Chem. Rev.* **1993**, *125*, 283−292.
(12) Evans, W. J.; Drummond, D. K. *Organometallics* **1988**, *7*, 797−802.
(13) Davies, J. A.; Hartley, F. R.; Murray, S. G.; Pierce-Butler, M. A. *J. Chem. Soc., Dalton Trans.* **1983**, 1305−1308.
(14) Martinez, J.; Adams, H.; Bailey, N. A.; Maitlis, P. M. *J. Organomet. Chem.* **1991**, *405*, 393−402.
(15) Schinnerling, P.; Thewalt, U. *J. Organomet. Chem.* **1992**, *431*, 41−45.
(16) Oshio, H.; Yamamoto, M.; Ito, T. *Inorg. Chem.* **2002**, *41*, 5817−5820.

10.1021/ja035253h CCC: $25.00

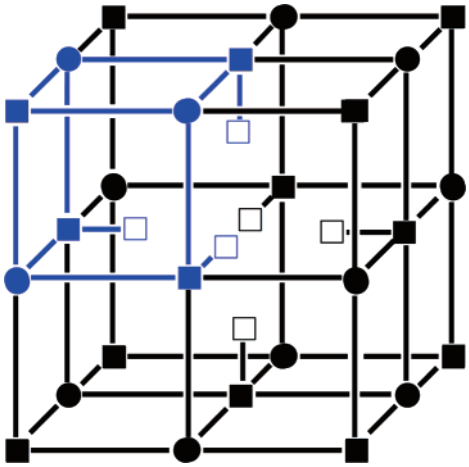

Figure 1. Unit cell for Prussian Blue, $Fe_4[Fe(CN)_6]_3 \cdot 3(H_2O)_6$, as proposed by Ludi et al.[25] ■, Fe(III) (N and O coordination); ●, Fe(II) (C coordination); and □, H_2O. The blue highlighted area represents a defect box subunit.

framework of which defines a series of boxlike subunits (Figure 1). As indicated by its formula, PB consists of many defects, and these defects are integrally related to PB's host−guest behavior.[26,27] Thus, whereas $(LM)_8(CN)_{12}$ cages have been mentioned as molecular representations of PB,[28] lower symmetry derivatives of such cubic cages in fact would be more faithful representations of PB, with regards to both structure and function. Such a defect structure provides context for the present project, which describes a series of heptametallic cyano-bridged cages. PB and some of its analogues exhibit a particular affinity for Cs^+.[29] Improved understanding of cyanometalate−Cs^+ interactions provides a second context for our work, that is, the design of new classes of ion selection agents.[30,31]

In prior work, the 1:1 reaction of $[CpCo(CN)_3]^-$ and $[Cp^*Rh(NCMe)_3]^{2+}$ was shown to afford $\{[CpCo(CN)_3]_4[Cp^*Rh]_4\}^{4+}$. This boxlike cage has a van der Waals' void volume of ca. 54 Å^3.[19] Subsequently, we found that the related reaction involving $[Cp^*Rh(CN)_3]^-$ in place of $[CpCo(CN)_3]^-$ affords the C_{3v} symmetric cage $\{[Cp^*Rh(CN)_3]_4[Cp^*Rh]_3\}^{2+}$, referred to in this paper as a "defect box" due to its structural similarity to the parent molecular boxes (Scheme 1).[32]

The following lessons were learned from our initial studies on Cp^*Rh^{2+}-based cages:

Scheme 1

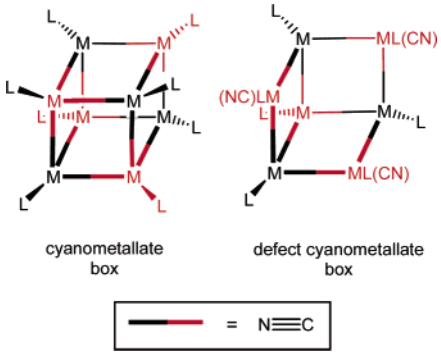

(1) Cationic cages failed to exhibit detectable host−guest behavior. This finding led to our interest in anionic or charge-neutral cages.

(2) The stoichiometry of the condensing partners significantly influences the course of the condensation.

(3)The steric bulk of the ancillary ligands (e.g., Cp vs Cp*) can be used to modify the box-forming tendencies of these cyanometalates. Because of the relative stereochemistry of the three terminal cyanide ligands (CN_t) in defect cages, their M_7-CN_{12} frameworks are not true subunits of the completed M_8-$(CN)_{12}$ boxes. Addition of $[Cp^*Rh(NCMe)_3]^{2+}$ to $\{[Cp^*Rh(CN)_3]_4[Cp^*Rh]_3\}^{2+}$ does not lead to cage closure.

(4) The M−CN−M′ linkages are ordered in all known cyanometalate boxes and defect boxes, as shown by ^{13}C NMR and crystallographic studies. Metals with labile M−CN linkages do not form box or defect-box structures.[33,34]

These four points underpin the present study, which originated with our recently reported synthesis of $[CpCo(CN)_3]^-/[Cp^*Ru]^+$ cages.[35] These Co−Ru cages, which are less cationic than related Cp^*Rh^{2+} derived species, require the presence of a templating cation, Cs^+ being particularly versatile in this regard. We found that the $[CpCo(CN)_3]^-/[Cp^*Ru]^+/Cs^+$ reaction affords both Cs⊂M_7 defect boxes and Cs⊂M_8 boxes, depending on the reaction stoichiometry.[35] We confirmed that Cs⊂$[CpCo(CN)_3]_4[Cp^*Ru]_4^+$ (**Cs⊂Co$_4$Ru$_4^+$**)[35] adopts the boxlike structure anticipated by its more labile analogue $\{Cs\subset[Cp^*Rh(CN)_3]_4[Mo(CO)_3]_4\}^{3-}$.[24] The structure of the defect box Cs⊂$[CpCo(CN)_3]_4[Cp^*Ru]_3$ (**Cs⊂Co$_4$Ru$_3$**), however, is of great interest because it was unclear exactly how the Cs^+ was accommodated by the CN_t (terminal) ligands. NMR studies indicated that **Cs⊂Co$_4$Ru$_3$** exists as a mixture of two unsymmetrical isomers, which were proposed to differ in terms of the relative stereochemistry of the Cp and CN_t ligands on the "rim" of the cage (Figure 2). The structure proposed for **Cs⊂Co$_4$Ru$_3$** was unprecedented because it involved terminal CN ligands π-bonded to Cs^+. Interest in this cage was enhanced because, despite its existence as isomers, it behaves as a tridentate ligand, somewhat akin to trispyrazoyl borates, triazacyclononane, etc., enabling the formation of novel heterotrimetallic boxes and double boxes (Scheme 2).

The defect boxes represent a novel motif for ion sequestration, as they possess a pocket for guest ions.[28] Whereas the ion exchange rates for the guest in **guest⊂M$_4$M$_4$** are quite slow,[28]

(17) Obora, Y.; Ohta, T.; Stern, C. L.; Marks, T. J. *J. Am. Chem. Soc.* **1997**, *119*, 3745−3755.
(18) Heinrich, J. L.; Berseth, P. A.; Long, J. R. *Chem. Commun.* **1998**, 1231−1232.
(19) Klausmeyer, K. K.; Rauchfuss, T. B.; Wilson, S. R. *Angew. Chem., Int. Ed.* **1998**, *37*, 1694−1696.
(20) Beauvais, L. G.; Shores, M. P.; Long, J. R. *Chem. Mater.* **1998**, *10*, 3783−3786.
(21) Beauvais, L. G.; Shores, M. P.; Long, J. R. *J. Am. Chem. Soc.* **2000**, *122*, 2763−2772.
(22) Holmes, S. M.; Girolami, G. S. *J. Am. Chem. Soc.* **1999**, *121*, 5593−5594.
(23) Beauvais, L. G.; Long, J. R. *J. Am. Chem. Soc.* **2002**, *124*, 12096−12097.
(24) Klausmeyer, K. K.; Wilson, S. R.; Rauchfuss, T. B. *J. Am. Chem. Soc.* **1999**, *121*, 2705−2711.
(25) Herren, F.; Fischer, P.; Ludi, A.; Haelg, W. *Inorg. Chem.* **1980**, *19*, 956−959.
(26) Lundgren, C. A.; Murray, R. W. *Inorg. Chem.* **1988**, *27*, 933−939.
(27) Pyrasch, M.; Toutianoush, A.; Jin, W.; Schnepf, J.; Tieke, B. *Chem. Mater.* **2003**, *15*, 245−254.
(28) Sodio, C. N. H.; Ramesh, M.; Espenson, J. H.; Rauchfuss, T. B. *Angew. Chem., Int. Ed.* **2003**.
(29) Dunbar, K. R.; Heintz, R. A. *Prog. Inorg. Chem.* **1997**, *45*, 283−391.
(30) Bryan, J. C.; Kavallieratos, K.; Sachleben, R. A. *Inorg. Chem.* **2000**, *39*, 1568−1572.
(31) Gokel, G. W.; Barbour, L. J.; Ferdani, R.; Hu, J. *Acc. Chem. Res.* **2002**, *35*, 878−886.
(32) Contakes, S. M.; Klausmeyer, K. K.; Milberg, R. M.; Wilson, S. R.; Rauchfuss, T. B. *Organometallics* **1998**, *17*, 3633−3635.
(33) Contakes, S. M.; Rauchfuss, T. B. *Angew. Chem., Int. Ed.* **2000**, *39*, 1984−1986.
(34) Contakes, S. M.; Rauchfuss, T. B. *Chem. Commun.* **2001**, 553−554.
(35) Contakes, S. M.; Kuhlman, M. L.; Ramesh, M.; Wilson, S. R.; Rauchfuss, T. B. *Proc. Natl. Acad. Sci. U.S.A.* **2002**, *99*, 4889−4893.

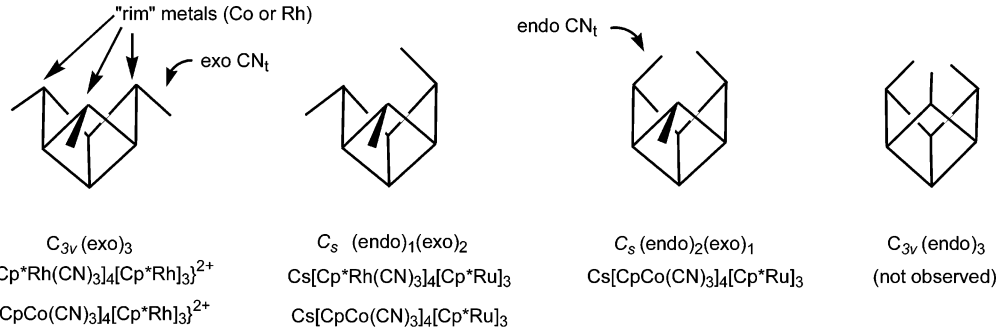

Figure 2. Structural isomers of $(LM)_7(\mu\text{-}CN)_9(CN_t)_3$ cages where the lines indicate the CN ligands.

Scheme 2

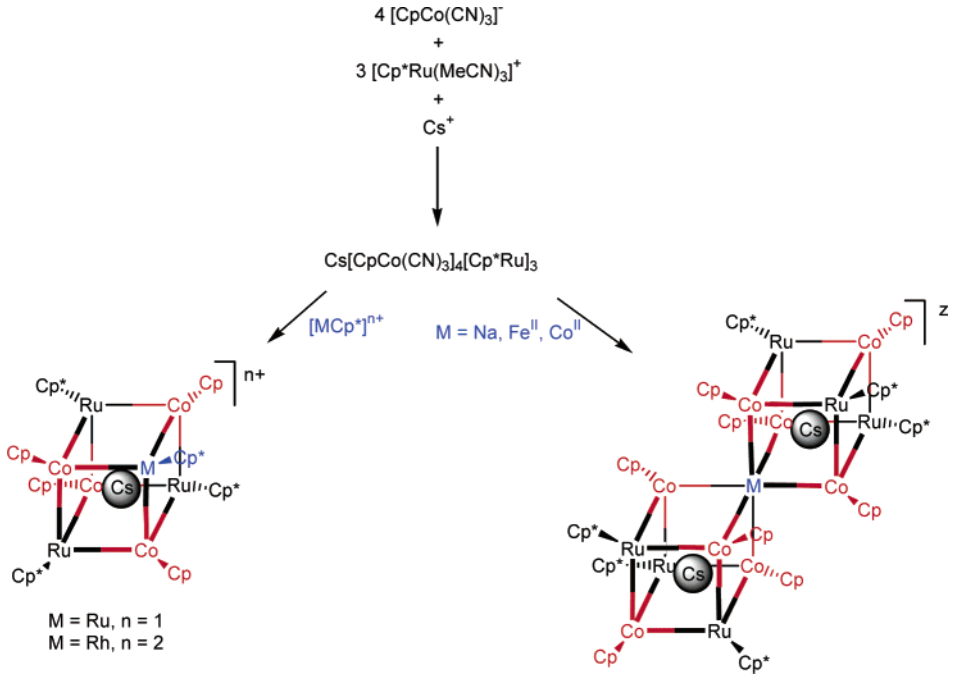

the ion exchange rates for the defect boxes should be high because of their more open structure. This motif is potentially relevant to the design of new sequestering agents for radiowaste materials.[36,37]

Results and Discussion

I. Synthesis and Reactivity. Synthesis and Characterization of {Cs⊂[Cp*Rh(CN)$_3$]$_4$[Cp*Ru]$_3$}. Reaction of 0.75 equiv of $[Cp^*Ru(NCMe)_3]PF_6$ with $Et_4N[Cp^*Rh(CN)_3]$ and 0.25 equiv of CsOTf in MeCN solution produced {Cs⊂[Cp*Rh(CN)$_3$]$_4$-[Cp*Ru]$_3$} (**Cs⊂Rh$_4$Ru$_3$**). Golden yellow crystals of the product were obtained in excellent yield (eq 2).

$$3[Cp^*Ru(NCMe)_3]^+ + 4[Cp^*Rh(CN)_3]^- + M^+ \rightarrow M\subset[Cp^*Rh(CN)_3]_4[Cp^*Ru]_3 \quad (\mathbf{M\subset Rh_4Ru_3},\ M = Cs,\ NH_4) \qquad (2)$$

The IR spectrum of **Cs⊂Rh$_4$Ru$_3$** features ν_{CN} bands at 2158, 2142, 2124, and 2121 cm^{-1}, which are shifted to higher frequencies versus 2124 and 2114 cm^{-1} for free $(Et_4N)[Cp^*Rh(CN)_3]$. ESI-MS measurements confirmed the formula (m/z = 2107 amu). Signals were not detected for the corresponding box **Cs⊂Rh$_4$Ru$_4$**$^+$. Purified samples of **Cs⊂Rh$_4$Ru$_3$** proved unreactive toward additional $[Cp^*Ru(NCMe)_3]^+$. Consequently, the stoichiometry of the reaction in eq 2 is not as critical as the synthesis of {Cs⊂[CpCo(CN)$_3$]$_4$[Cp*Ru]$_3$}.[28]

Attempted syntheses of the empty (or voided) anionic bowl $\{[Cp^*Rh(CN)_3]_4[Cp^*Ru]_3\}^-$ were unsuccessful. Reaction of 0.75 equiv of $[Cp^*Ru(NCMe)_3]PF_6$ with $(Et_4N)[Cp^*Rh(CN)_3]$ resulted in insoluble solids. Such negative results, which are reminiscent of the untemplated reactions of $[Cp^*Ru(NCMe)_3]^+$ and $[CpCo(CN)_3]^-$,[35] underscore the important role of the Cs^+ template.

ESI-MS Studies on Cage Assembly. In contrast to **Cs⊂Co$_4$Ru$_3$**, the all-Cp* cage **Cs⊂Rh$_4$Ru$_3$** exhibits good solubility in MeCN despite the fact that it is charge-neutral. This property enabled us to monitor the cage-forming process by ESI-MS measurements on homogeneous MeCN solutions. Analysis of the crude reaction mixture by ESI-MS was hindered by the presence of Et_4NPF_6, which dominates the ion current. ESI-MS analysis of reaction mixtures revealed no anionic cage intermediates in the cage formation process − only PF_6^- was

(36) Sachleben, R. A.; Urvoas, A.; Bryan, J. C.; Haverlock, T. J.; Moyer, B. A.; Hay, B. P. *Chem. Commun.* **1999**, 1751−1752.

(37) Casnati, A.; Pochini, A.; Ungaro, R.; Ugozzoli, F.; Arnaud, F.; Fanni, S.; Schwing, M.-J.; Egberink, R. J. M.; de Jong, F.; Reinhoudt, D. N. *J. Am. Chem. Soc.* **1995**, *117*, 2767−2777.

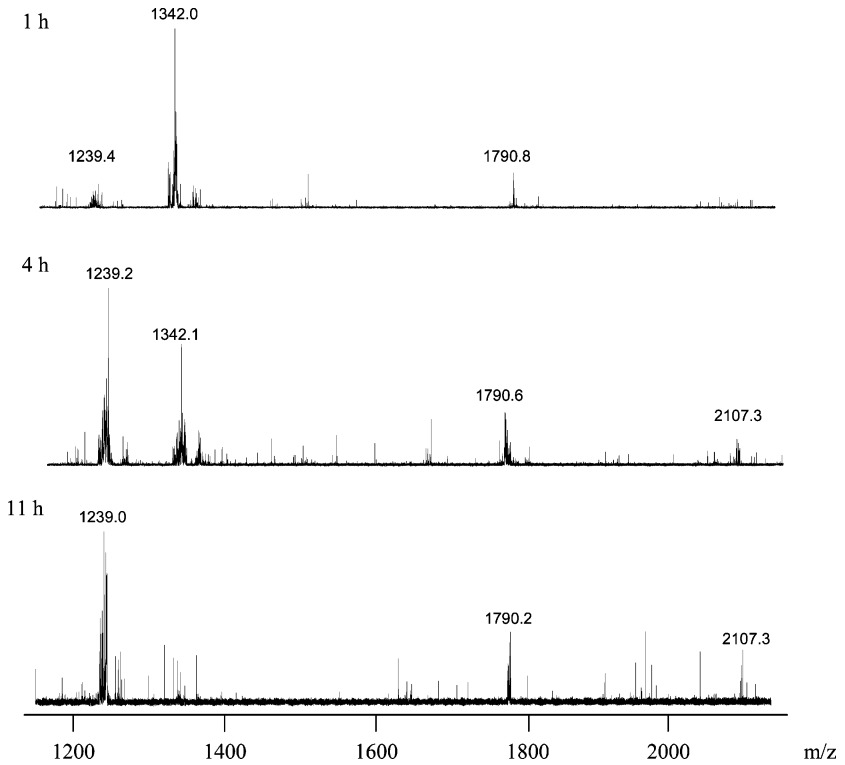

Figure 3. ESI-MS spectra at 1, 4, and 11 h for the reaction of 0.25 equiv of Cs^+, $Cp^*Rh(CN)_3^-$, and 0.75 equiv of $Cp^*Ru(MeCN)_3^+$ leading ultimately to the formation of **Cs⊂Rh$_4$Ru$_3$**. Assignments: **Cs⊂Rh$_2$Ru$_2^+$** (1239 *m*/*z*), **Rh$_2$Ru$_3^+$** (1342 *m*/*z*), **Cs⊂Rh$_3$Ru$_3^+$** (1791 *m*/*z*), as well as the product, **Cs⊂Rh$_4$Ru$_3$** (2107 *m*/*z*).

observed. Under normal synthesis conditions, the formation of **Cs⊂Rh$_4$Ru$_3$** requires 24 h, and, during this time, three intermediates were observed, **Cs⊂Rh$_2$Ru$_2^+$** (1239 amu), **Rh$_2$Ru$_3^+$** (1342 amu), **Cs⊂Rh$_3$Ru$_3^+$** (1791 amu), as well as the product [**Cs⊂Rh$_4$Ru$_3$**] (2107 amu). The first product to appear is **Rh$_2$Ru$_3^+$** (Figure 3). Over the course of hours, this intermediate is consumed concomitant with the appearance of both **Cs⊂Rh$_2$Ru$_2^+$** and **Cs⊂Rh$_3$Ru$_3^+$**, as well as the final product. Monitoring the reaction revealed that the amount of final product increased concomitant with the decrease in the proposed intermediates, suggesting they are true intermediates and not a side product of the reaction. MS/MS measurements showed that these cations do not arise from fragmentation of **Cs⊂Rh$_4$Ru$_3$**. ESI-MS analysis revealed that "NMR-pure" samples of **Cs⊂Rh$_4$Ru$_3$** contain trace impurities of **Cs⊂Rh$_2$Ru$_2^+$** and **Cs⊂Rh$_3$Ru$_3^+$**, which can be removed by further recrystallization. This fact indicates that these smaller cages may in fact be isolable, although this was not explored.

The admittedly limited ESI-MS data can be rationalized in the context of a tentative mechanism for the formation of **Cs⊂Rh$_4$Ru$_3$**. An initially formed charge-neutral square **Rh$_2$Ru$_2$**, which would not be easily detected by ESI-MS, would bear terminal CN ligands attractive toward Cp^*Ru^+ centers. The resulting **Rh$_2$Ru$_3^+$** apparently undergoes an exchange process of Cp^*Ru^+ for Cs^+ leading to **Cs⊂Rh$_2$Ru$_2^+$**. Thereafter, the cage growth process is proposed to follow an alternating addition of anionic $[Cp^*Rh(CN)_3]^-$ and cationic Cp^*Ru^+ centers. One clear conclusion from these measurements is that Cs^+ participates in the early stages of cage assembly.

^{133}Cs NMR Measurements. ^{133}Cs NMR spectroscopy provided a useful tool for characterizing these Cs-containing cage compounds. Not only do the spectra allow one to assay the purity of cage samples, the chemical shift was found to correlate with the number of η^2-CN ligands surrounding the Cs^+ ion (Figure 4). **Cs⊂Co$_4$Ru$_4^+$** with all 12 cyanides interacting with Cs^+ resulted in a signal at δ 1 versus δ 34 for CsOTf, which we attribute to maximal shielding relative to the other cases. In **Cs⊂Rh$_4$Ru$_3$**, where Cs^+ is surrounded by only 10 CN ligands, the ^{133}Cs signal occurs at δ 91. Key interpolations come from measurements on **Cs⊂Co$_4$Ru$_3$**, which consists of two isomers, one of which has 11 CN ligands interacting with Cs^+ and the other with 10 (vide infra). The dominant signal at δ 42 is assigned as the isomer with a $Cs(CN)_{11}$ site, that is, the isomer that crystallizes (allowing us to assign the ^{1}H NMR signals to particular isomers). The minor signal (δ 89) is assigned to the isomer with a $Cs(CN)_{10}$ site, as for **Cs⊂Rh$_4$Ru$_3$**. The ^{133}Cs MAS NMR spectrum for a solid sample of **Cs⊂Rh$_4$Ru$_3$** was inconclusive, showing one broad peak within the range of both isomers (δ 63).

{NH$_4$⊂[Cp*Rh(CN)$_3$]$_4$[Cp*Ru]$_3$}. The fact that the voided cage **[Rh$_4$Ru$_3$]$^-$** could not be synthesized indicates that complexation to cations is important for cage stability, as well as cage formation (see above). On the basis of our inability to synthesize **K⊂Rh$_4$Ru$_3$**, we concluded that K^+ (r_{ionic} = 1.52 Å) is too small. In contrast, NH_4^+ (r_{ionic} = 1.75 Å), which is only 0.06 Å smaller than Cs^+, does template the formation of a defect box. The addition of 0.75 equiv of $[Cp^*Ru(NCMe)_3]^+$ to a MeCN solution of $Et_4N[Cp^*Rh(CN)_3]$ in the presence of 0.25 equiv of NH_4PF_6 efficiently produced $NH_4⊂[CpCo(CN)_3]_4$-$[Cp^*Ru]_3$ (**NH$_4$⊂Rh$_4$Ru$_3$**, eq 2). ESI-MS measurements confirmed the formula, with M^+ at m/z = 1992 amu. With regards to the less hindered cages, we have been unable to synthesize **M⊂Co$_4$Ru$_3$** for any M other than Cs.

The IR spectrum of **NH$_4$⊂Rh$_4$Ru$_3$** in the ν_{NH} region indicated

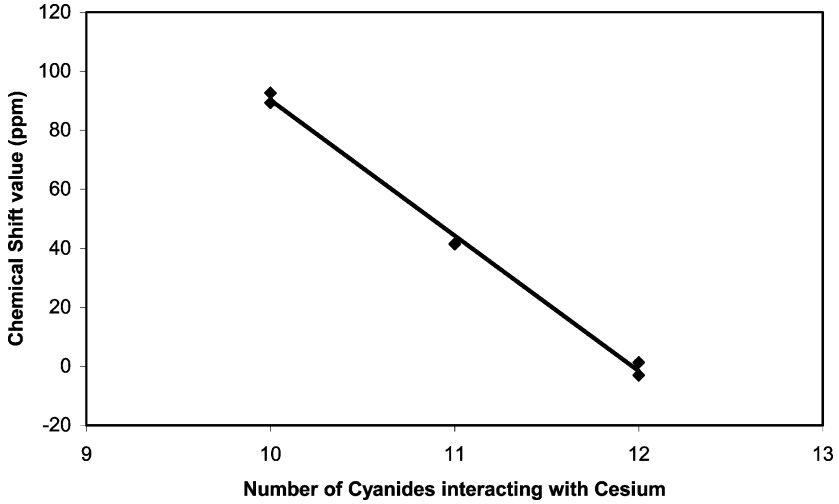

Figure 4. Plot of ^{133}Cs NMR chemical shift vs number of π-CN^- ligands interacting with the Cs^+. Data: **Cs⊂Co$_4$Ru$_4$**$^+$ (δ 1), two isomers of **Cs⊂Co$_4$Ru$_3$** (δ 89 for minor isomer, 42 for major isomer), **Cs⊂Rh$_4$Ru$_3$** (δ 91), and Cs⊂{[Cp*Rh(CN)$_3$]$_4$[Mo(CO)$_3$]$_4$}$^{3-}$ ($-\delta$ 3).

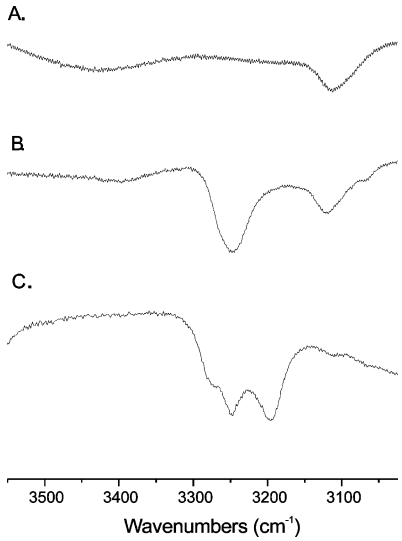

Figure 5. IR spectra (KBr pellets) in the ν_{NH} region for **Co$_4$Ru$_4$** (A) as a blank, **NH$_4$⊂Co$_4$Ru$_4$**$^+$ (B),[28] and **NH$_4$⊂Rh$_4$Ru$_3$** (C).

that the cation is bound in an unsymmetrical environment. Peaks were observed at 3196, 3246, and 3270 (sh) cm^{-1}. In contrast, the IR spectrum of **NH$_4$⊂Co$_4$Ru$_4$**$^+$ shows only one peak at 3250 cm^{-1} assigned to the T_2 mode reflecting a symmetrical environment (Figure 5). In **NH$_4$⊂Rh$_4$Ru$_3$**, the T_2 mode has split into E and A_1 modes, while the A_1, previously only Raman-active, becomes IR-active due to the decreased site symmetry.[38] This low site symmetry arises not only from the overall cage structure, but more specifically from the unique N−H···NC interaction between the endo CN_t and one of four NH bonds (vide infra). Typical strong X···HNH$_3^+$ hydrogen bonds exhibit two energetically distinct ν_{N-H} bands. Isolated N−H units exhibit $\nu_{N-H} \approx 3400-3260$ cm^{-1}, whereas for N−H···X-containing species $\nu_{N-H} \approx 2975-3110$ cm^{-1}.[39] For **NH$_4$⊂Rh$_4$Ru$_3$**, $\Delta\nu_{NH} = 50$ cm^{-1}, which indicates a weak interaction between NH_4^+ and the π-bond of CN_t. The T_2 bending mode of NH_4^+ is obscured by the ν_{C-H} bands for the facially capping Cp and Cp* ligands at 1600−1200 cm^{-1}.

(38) Zecchina, A.; Marchese, L.; Bordiga, S.; Paze, C.; Gianotti, E. *J. Phys. Chem. B* **1997**, *101*, 10128−10135.
(39) Sauer, J.; Ugliengo, P.; Garrone, E.; Saunders, V. R. *Chem. Rev.* **1994**, *94*, 2095−2160.

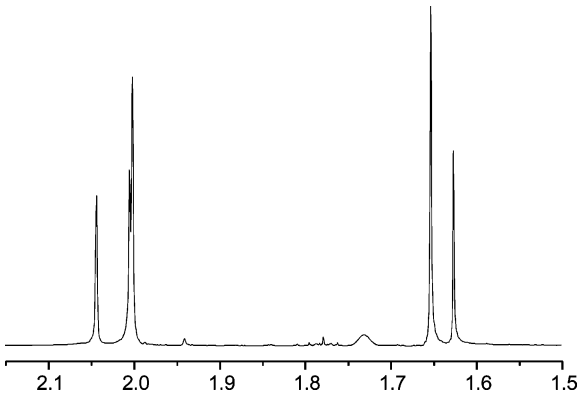

Figure 6. 500 MHz ^{1}H NMR spectrum of **NH$_4$⊂Rh$_4$Ru$_3$** (THF solution). The 1:1:2 Cp*Rh and 2:1 Cp*Ru patterns are consistent with one C_s isomer.

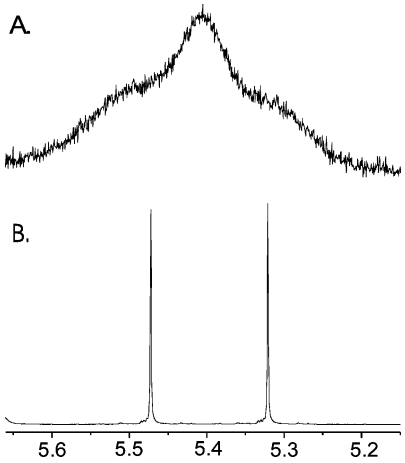

Figure 7. 500 MHz ^{1}H NMR spectrum of the NH_4^+ region for unenriched **NH$_4$⊂Rh$_4$Ru$_3$** (A) and **^{15}NH$_4$⊂Rh$_4$Ru$_3$** (B) in THF solutions.

As for **Cs⊂Rh$_4$Ru$_3$**, **NH$_4$⊂Rh$_4$Ru$_3$** exists as one isomer in MeCN solution as shown by ^{1}H NMR spectroscopy (Figure 6). A broad multiplet is observed at δ 5.40 for the NH_4^+ signal. The ^{1}H NMR spectrum of **^{15}NH$_4$⊂Rh$_4$Ru$_3$** exhibits a doublet at δ 5.40, demonstrating that the cation is tumbling fast on the NMR time scale inside of the cage (Figure 7). In MeCN solutions, **NH$_4$⊂Rh$_4$Ru$_3$** undergoes rapid exchange H−D exchange with D_2O, demonstrating that the ammonium ion is

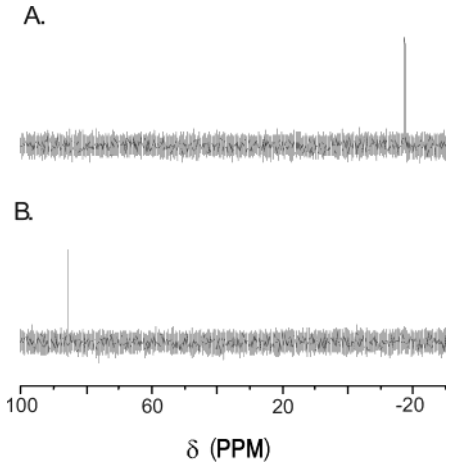

Figure 8. 76 MHz ^{133}Cs NMR spectrum of $[Cs(BCB6)]^+$ (in MeCN solution) before (A) and after (B) treatment with 1 equiv of $\mathbf{NH_4{\subset}Rh_4Ru_3}$. The δ 88 signal corresponds to $\mathbf{Cs{\subset}Rh_4Ru_3}$.

highly accessible to the solution. Similar experiments show that $\mathbf{NH_4{\subset}Co_4Ru_4}^+$ is unreactive toward H−D exchange under these conditions, reflecting the chemical shielding afforded by the completed box.[28] Addition of CsOTf to a MeCN solution of $\mathbf{NH_4{\subset}Rh_4Ru_3}$ quantitatively affords $\mathbf{Cs{\subset}Rh_4Ru_3}$ within 20 min.

Affinity of $\mathbf{NH_4{\subset}Rh_4Ru_3}$ for Cs^+. The affinity of $\mathbf{NH_4{\subset}Rh_4Ru_3}$ for Cs^+ was qualitatively examined in a competition experiment using calix[4]arene-bis(benzocrown-6) (**BC6B**, Figure 8), a representative member for high-affinity ($K_{eq} = 10^6$) cesium-selective calix[4]arene-crown-6 ligands.[40−44] A MeCN solution of $[Cs(BC6B)]^+$ (^{133}Cs NMR: $-\delta$ 17) was treated with 1 equiv of $\mathbf{NH_4{\subset}Rh_4Ru_3}$, resulting within the time required for NMR analysis in quantitative conversion to $\mathbf{Cs{\subset}Rh_4Ru_3}$ (δ 88, see eq 3, Figure 8). The Cs^+/K^+ and Cs^+/Na^+ selectivities have not been determined, but our inability to synthesize $\mathbf{K{\subset}Rh_4Ru_3}$ suggests these selectivity values are quite high.

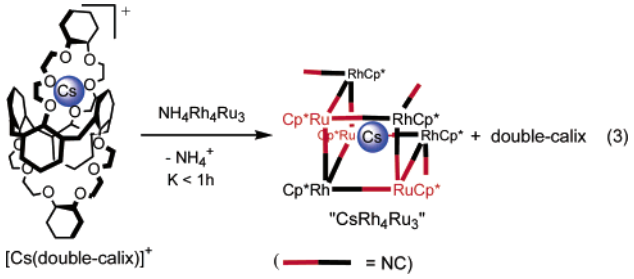

II. Structural Analyses. Isomerism in the Defect Boxes. Defect boxes could, in principle, adopt four isomeric structures, depending on the relative orientation of the three CN_t ligands (see Figure 2). ^{1}H NMR measurements show that $\mathbf{Cs{\subset}Rh_4Ru_3}$ exists as one of the two C_s isomers, as demonstrated by the observation of five Cp* signals in a ratio 1:1:2:2:1. In contrast,

(40) Haverlock, T. J.; Mirzadeh, S.; Moyer, B. A. *J. Am. Chem. Soc.* **2003**, *125*, 1126−1127.
(41) Casnati, A.; Sansone, F.; Dozol, J.-F.; Rouquette, H.; Arnaud-Neu, F.; Byrne, D.; Fuangswasdi, S.; Schwing-Weill, M.-J.; Ungaro, R. *J. Inclusion Phenom. Macrocyclic Chem.* **2001**, *41*, 193−200.
(42) Lamare, V.; Dozol, J.-F.; Fuangswasdi, S.; Arnaud-Neu, F.; Thuéry, P.; Nierlich, M.; Asfari, Z.; Vicens, J. *J. Chem. Soc., Perkin Trans. 2* **1999**, 271−284.
(43) Lamare, V.; Dozol, J.-F.; Ugozzoli, F.; Casnati, A.; Ungaro, R. *Eur. J. Org. Chem.* **1998**, 1559−1568.
(44) Thuéry, P.; Nierlich, M.; Bryan, J. C.; Lamare, V.; Dozol, J.-F.; Asfari, Z.; Vicens, J. *J. Chem. Soc., Dalton Trans.* **1997**, 4191−4202.

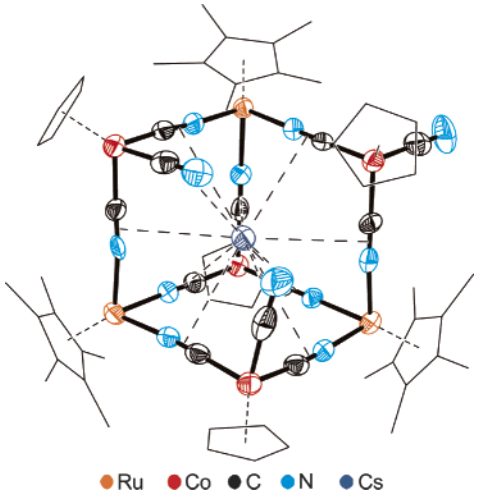

Figure 9. Molecular structure of $\mathbf{Cs{\subset}[CpCo(CN)_3]_4[Cp^*Ru]_3}$ showing the atom labeling scheme. Thermal ellipsoids are drawn at the 50% level.

Scheme 3

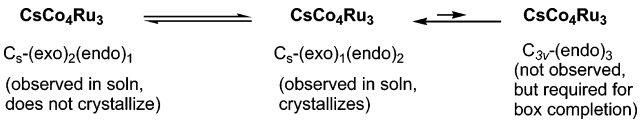

^{1}H NMR spectra for solutions of $\mathbf{CsCo_4Ru_3}$ reveal the presence of two unsymmetrical (C_s) isomers, each of which show characteristic subspectra, which can now be assigned on the basis of the ^{133}Cs NMR data (see above). ^{1}H NMR experiments (−60 to 60 °C) did not reveal any line-broadening. If coalescence temperature is conservatively estimated to be 20 °C above 60 °C, this would imply that the rate constant for exo−endo isomerization would have an upper limit of 50 s^{-1}. In solution, the cage $\mathbf{CsCo_4Ru_3}$ is rapidly capped (box-completion reaction) with various electrophiles,[35] such as Na^+ and Cp^*Rh^{2+}, and this process is complete within minutes at room temperature (the time required to prepare sample for NMR analysis). Assuming that the rate of complexation is determined by the unimolecular rate of exo−endo isomerization, the speed of the box completion reaction indicates that the speed of the exo−endo isomerization is 0.05 s^{-1}.

The ^{1}H NMR spectrum of a solution freshly prepared from single crystals of $\mathbf{Cs{\subset}Co_4Ru_3}$ revealed the presence of the same two C_s isomers in the equilibrium ratio. The rapid isomerization of the cage is related to the ease with which it undergoes box-completion reactions.[35]

The dynamic structure of $\mathbf{Cs{\subset}Co_4Ru_3}$ is evident from the fact that we only isolate one isomer when we can observe two in solution. Furthermore, the facility with which this cage undergoes box-completion reactions implies that all three CN_t ligands can transiently, at least, adopt the all-endo geometry, thereby presenting incoming electrophiles with a tridentate ligand. These assumptions and facts can be accommodated by a mechanism of isomerization that involves the $C_s-C_{3v}-C_s$ process shown in the Scheme 3. An alternative mechanism is that the electrophile caps the C_s-(exo)$_1$(endo)$_2$ isomer and then isomerization occurs resulting in the C_{3v} product.

Crystallographic Analysis of $\{\mathbf{Cs{\subset}[CpCo(CN)_3]_4[Cp^*Ru]_3}\}$. Crystallographic characterization of $\mathbf{Cs{\subset}Co_4Ru_3}$ showed that it crystallizes as the C_s-(exo)$_1$(endo)$_2$ isomer (Figure 9, Table 1). Thus, although the ^{1}H and ^{133}Cs NMR data (see above)

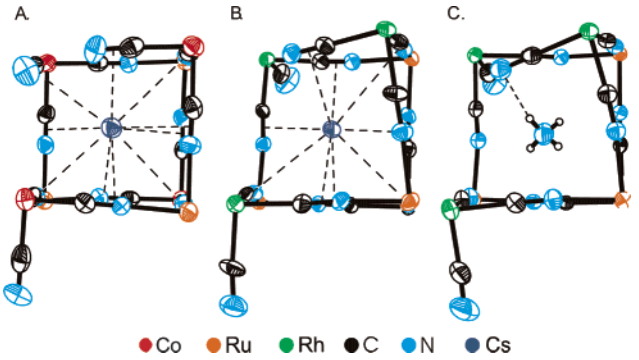

Figure 10. The view is approximately parallel to two of the $Co_2Rh_2(CN)_4$ faces so as to show the outward or inward bending of the terminal $M(CN)_3$ units (M = Co, Rh). (A) **Cs⊂Co$_4$Ru$_3$**, (B) **Cs⊂Rh$_4$Ru$_3$**, (C) **NH$_4$⊂Rh$_4$Ru$_3$**.

Table 1. Selected Bond Distances (Å) for the Cations in **Cs⊂Co$_4$Ru$_3$** and **Cs⊂Rh$_4$Ru$_3$**

parameter	Cs⊂Co$_4$Ru$_3$	Cs⊂Rh$_4$Ru$_3$
C(1)−Cs(1)	3.651(8)	3.512(14)
C(2)−Cs(1)	3.704(8)	3.451(14)
C(3)−Cs(1)	3.661(8)	3.540(15)
C(4)−Cs(1)	3.647(8)	exo-CN$_t$
C(5)−Cs(1)	3.767(8)	3.821(16)
C(6)−Cs(1)	3.729(8)	3.748(16)
C(7)−Cs(1)	exo-CN$_t$	3.644(14)
C(8)−Cs(1)	3.517(7)	3.919(16)
C(9)−Cs(1)	3.567(8)	exo-CN$_t$
C(10)−Cs(1)	3.864(8)	3.700(15)
C(11)−Cs(1)	3.551(8)	3.641(14)
C(12)−Cs(1)	3.606(9)	3.402(15)
N(1)−Cs(1)	3.526(6)	3.525(12)
N(2)−Cs(1)	3.677(6)	3.357(12)
N(3)−Cs(1)	3.587(6)	3.580(12)
N(4)−Cs(1)	3.518(6)	exo-CN$_t$
N(5)−Cs(1)	3.665(7)	3.532(12)
N(6)−Cs(1)	3.649(8)	3.603(13)
N(7)−Cs(1)	exo-CN$_t$	3.344(12)
N(8)−Cs(1)	3.552(6)	3.795(13)
N(9)−Cs(1)	3.598(6)	exo-CN$_t$
N(10)−Cs(1)	3.871(9)	3.715(13)
N(11)−Cs(1)	3.470(6)	3.579(12)
N(12)−Cs(1)	3.433(9)	3.250(13)

indicated the presence of both C_s isomers in solution, only one isomer crystallizes. Three types of Cp*Co(CN)$_3$ centers are observed in a 1:1:2 ratio as well as two types of Cp*Ru centers. Nine of the twelve CN ligands form Co−CN−Ru bridges; the remaining three CN groups are terminal with two endo and one exo. The endo CN$_t$ groups interact with Cs$^+$, with average N$_t$···Cs and C$_t$···Cs distances of 3.56 and 3.67 Å, respectively. The nine μ-CN ligands are slightly less strongly bound to Cs$^+$ with Cs···N distances (3.61 Å) again being shorter than the C···Cs distances (3.66 Å),[45] although it appears that the CN$_t$ is slightly more strongly bound to Cs than is μ-CN. Typical Cs···NC distances range from 3.113 to 3.678 Å[46,47] with an average distance of 3.28 ± 0.16 Å.[48] With respect to distortions of the overall $M_7(CN)_{12}$ framework, the $Co_2Ru_2(CN)_4$ face bearing the exo-CN is slightly bowed inward (Figure 10). The extent of this distortion is indicated by the Co···Co distances within the

(45) Williams, J. M.; Johnson, P. L.; Schultz, A. J.; Coffey, C. C. *Inorg. Chem.* **1978**, *17*, 834−839.
(46) Werner, B.; Kraeuter, T.; Neumueller, B. *Organometallics* **1996**, *15*, 3746−3751.
(47) Ponomareva, V. V.; Skopenko, V. V.; Domasevitch, K. V.; Sieler, J.; Gelbrich, T. *Z. Naturforsch., B: Chem. Sci.* **1997**, *52*, 901−905.
(48) Cambridge Structural Database version 5.24, search of Cs−NC distances (16 examples).

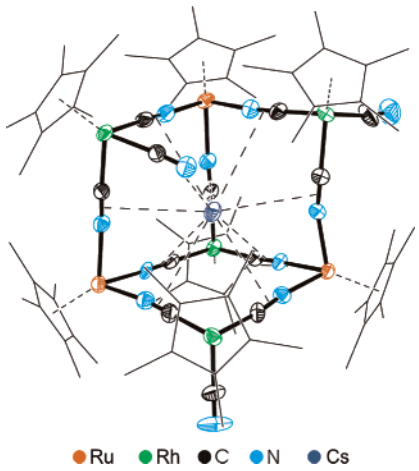

Figure 11. Molecular structure of **Cs⊂[Cp*Rh(CN)$_3$]$_4$[Cp*Ru]$_3$** showing the atom labeling scheme. Thermal ellipsoids are drawn at the 50% level.

Scheme 4

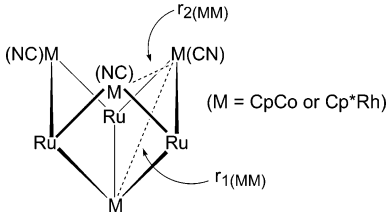

$Co_2Rh_2(CN)_4$ rings, defined as r_{1CoCo}, versus the Co···Co distances between the CpCo(CN$_t$) centers, defined as r_{2CoCo} (Scheme 4). Of the three r_{2CoCo} values, two are ∼0.16 Å (2.2%) shorter and one is 0.23 Å (3.2%) longer versus $(r_{1CoCo})_{avg}$.

Crystallographic Analysis of {Cs⊂[Cp*Rh(CN)$_3$]$_4$[Cp*Ru]$_3$}. Cs⊂Rh$_4$Ru$_3$ adopts the second C_s-(exo)$_2$(endo)$_1$ isomer − the one that did not crystallize for **Cs⊂Co$_4$Ru$_3$** (Figure 11, Table 1). For the endo CN$_t$, the N···Cs distance of 3.25 Å is ca. 0.11 Å shorter than the other nine N···Cs distances, which average 3.59 Å.[49] Similarly, the C···Cs distance of 3.40 Å is shorter than the other Cs···C distances, which average 3.67 Å. The bending of the Rh−C−N linkages in **Cs⊂Rh$_4$Ru$_3$** arises from the Cs···N distances again being ca. 0.10 Å shorter than the average Cs···C distance. The Cs atom is unsymmetrically situated with respect to the three Rh atoms at the rim of the defect box: Cs···Rh$_{rim}$(CN$_t$)$_{exo}$ = 4.77 Å versus Cs···Rh$_{rim}$(CN$_t$)$_{endo}$ = 4.41 Å, while the "nonrim" Rh has a Cs···Rh = 4.31 Å.

The metal cyanide framework of **Cs⊂Rh$_4$Ru$_3$** is more distorted than that in **Cs⊂Co$_4$Ru$_3$** resulting from two $Rh_2Ru_2(CN)_4$ faces being bowed outward, whereas the third face is significantly bowed inward (Figure 10). Using the metrical definitions described above, two r_{2RhRh} are 0.39 Å (5.2%) shorter and the one is 0.47 Å (6.3%) longer versus $(r_{1RhRh})_{avg}$.

Crystallographic Analysis of {NH$_4$⊂[Cp*Rh(CN)$_3$]$_4$[Cp*Ru]$_3$}. Of three cages described in this paper, **NH$_4$⊂Rh$_4$Ru$_3$** is the most distorted, reflecting the smaller ionic radius of NH$_4^+$ (Figure 12). The unique CN$_t$ is tilted toward the included cation, more so than in **Cs⊂Rh$_4$Ru$_3$** (Figure 13). This added tilting of the unique cyanide bows this **Rh$_2$Ru$_2$** face further inward, causing the other two faces to bow out further (Figure 10). From the above terminology, two r_{2RhRh} are 0.59 Å (7.9%) shorter,

(49) Johnson, P. L.; Koch, T. R.; Williams, J. M. *Acta Crystallogr., Sect. B* **1977**, *B33*, 1293−1295.

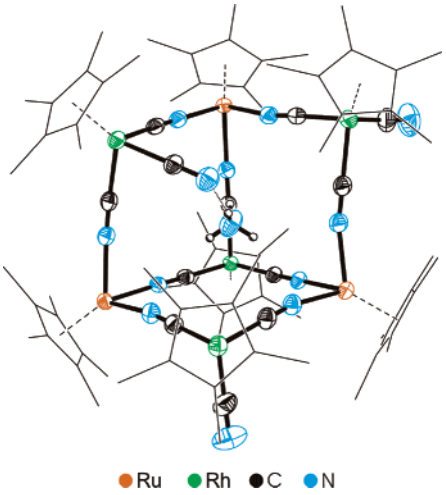

Figure 12. Molecular structure of **NH_4⊂[Cp*Rh(CN)$_3$]$_4$[Cp*Ru]$_3$** showing the atom labeling scheme. Thermal ellipsoids are drawn at the 50% level.

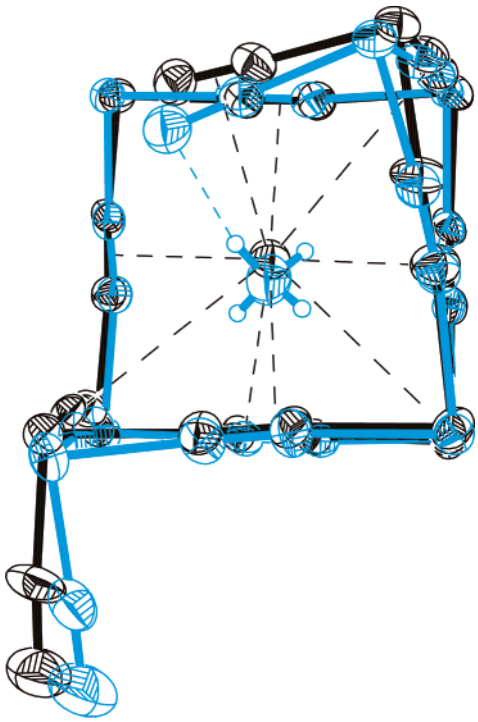

Figure 13. Overlay of **NH_4⊂Rh$_4$Ru$_3$** (blue) and **Cs⊂Rh$_4$Ru$_3$** (black).

while the unique r_{2RhRh} is 0.46 Å (6.1%) longer than $(r_{1RhRh})_{avg}$. The distortion is also evident in the comparison of Rh···N distances. The NH_4^+ is unsymmetrically situated with respect to the four Rh atoms: N···$Rh_{rim}(CN_t)_{exo}$ = 4.78 Å versus N···$Rh_{rim}(CN_t)_{endo}$ = 4.38 Å, while the "nonrim" Rh has a N···Rh = 4.14 Å. Thus, the cation in **NH_4⊂Rh$_4$Ru$_3$** is more deeply embedded into the $M_7(\mu\text{-CN})_9$ cavity (Figure 13).

The four protons of NH_4^+ were located with an average N−H distance of 0.80 Å. The H_4N···N_tC distance is 2.95 Å, and the H_3N−H···N_tC distance is 2.14 Å (Figure 12), which is typical of H_3N−H···N hydrogen bonds.[50−53] In contrast to **Cs⊂Rh$_4$Ru$_3$**, all three of the $M_4(CN)_4$ faces in [Cp*Rh(CN)$_3$]$_4$[Cp*Rh]$_3$(PF$_6$)$_2$ are significantly bowed outward, apparently due to repulsions between Cp*Rh(CN_t) centers. The $Ru_2Rh_2(CN_t)_{endo}$ face of **Cs⊂Rh$_4$Ru$_3$** is bowed inward toward Cs^+, arising from a short Cs···N distance of 3.25 (vs van der Waals radii for Cs···N, ∼3.3).

Summary

In this work, the structural chemistry of cation-containing defect cyanometalate boxes was elucidated. The less bulky derivative **Cs⊂Co$_4$Ru$_3$** is an interesting building block for new boxlike and double box cage structures.[35] The defect box also represents a promising motif for cation receptors because, unlike the corresponding completed boxes,[28] these cations are more solvent-accessible and hence more kinetically labile.

Specific conclusions follow:

(1) Whereas the first example of a defect box, [Cp*Rh(CN)$_3$]$_4$-[Cp*Rh]$_3^{2+}$, featured all exo-CN_t ligands,[32] the cation-containing defect boxes have one or two endo-CN_t ligands. These endo-CN_t ligands interact ionically with the guest cation.

(2) The steric profile of the coligands (Cp* vs Cp) allows one to enforce the defect box motif without box formation. Whereas **Cs⊂Co$_4$Ru$_3$** is reactive toward metal electrophiles to give boxlike cages, the all-Cp* species **Cs⊂Rh$_4$Ru$_3$** show no affinity for "capping" metal electrophiles.

(3) ^{133}Cs NMR spectroscopy provides a convenient indicator of the Cs^+ coordination environment in cyanometalates.

(4) The successful synthesis of **NH_4⊂Rh$_4$Ru$_3$** defines the dimensions critical for cage formation: NH_4^+ (r_{ionic} = 1.75 Å) being intermediate in size between K^+ (r_{ionic} = 1.52 Å), which does not react, and Cs^+ (r_{ionic} = 1.81 Å). **NH_4⊂Rh$_4$Ru$_3$** binds Cs^+ tightly and, in contrast to **NH_4⊂Co$_4$Ru$_4^+$**,[28] ion-exchanges rapidly.

(5) Structural analyses of the two defect boxes, **Cs⊂Co$_4$Ru$_3$**, **NH_4⊂Rh$_4$Ru$_3$**, and **Cs⊂Rh$_4$Ru$_3$**, reveal that cage distortion increases as the cationic guest becomes smaller or the Cp groups become larger.

(6) A competition experiment between a well-known cesium selective complexant demonstrates that **NH_4⊂Rh$_4$Ru$_3$** has a high affinity for cesium.

Materials and Methods

General. Standard Schlenk techniques were employed in all syntheses. Et$_4$N[Cp*Rh(CN)$_3$],[19] [Cp*Ru(NCMe)$_3$]PF$_6$,[54] {Cs⊂[CpCo(CN)$_3$]$_4$[Cp*Ru]$_3$},[35] CsOTf, and NH_4PF_6 were either prepared according to literature methods or purchased from Aldrich. Because the purity of [Cp*Ru(NCMe)$_3$]PF$_6$ proved critical, the as-synthesized salt was further recrystallized from CH_2Cl_2−Et_2O to give a bright yellow microcrystalline solid. Elemental analyses were conducted by the School of Chemical Sciences Microanalytical Laboratory. ^{13}C and ^{1}H NMR spectra were acquired on Varian Unity 400 and 500 NMR spectrometers. Infrared spectra were acquired on a Mattson Infinity Gold FTIR spectrometer using CaF_2 solution cells or with KBr pellets. Electrospray ionization-mass spectra (ESI-MS) and MS/MS measurements were acquired using a Micromass Quattro QHQ quadrupole−hexapole−quadrupole instrument.

Cs⊂[Cp*Rh(CN)$_3$]$_4$[Cp*Ru]$_3$ (Cs⊂Rh$_4$Ru$_3$). A solution of 384 mg (0.762 mmol) of purified [Cp*Ru(NCMe)$_3$]PF$_6$ in 20 mL of MeCN was added dropwise to a solution of 72 mg (0.254 mmol) of CsOTf and 457 mg (1.017 mmol) of Et$_4$N[Cp*Rh(CN)$_3$] in 25 mL of MeCN.

(50) Wallwork, S. C. *Acta Crystallogr.* **1962**, *15*, 758−759.
(51) Graf, E.; Kintzinger, J. P.; Lehn, J. M.; LeMoigne, J. *J. Am. Chem. Soc.* **1982**, *104*, 1672−1678.
(52) Johnson, P. L.; Schultz, A. J.; Underhill, A. E.; Watkins, D. M.; Wood, D. J.; Williams, J. M. *Inorg. Chem.* **1978**, *17*, 839−844.
(53) Virovets, A. V.; Fedin, V. P.; Samsonenko, D. G.; Clegg, W. *Acta Crystallogr., Sect. C: Cryst. Struct. Commun.* **2000**, *C56*, 272−273.
(54) Fagan, P. J.; Ward, M. D.; Calabrese, J. C. *J. Am. Chem. Soc.* **1989**, *111*, 1698−1719.

Table 2. Crystallographic Data for **Cs⊂Co$_4$Ru$_3$**, **Cs⊂Rh$_4$Ru$_3$**, and **NH$_4$⊂Rh$_4$Ru$_3$**

	Cs⊂Co$_4$Ru$_3$	Cs⊂Rh$_4$Ru$_3$	NH$_4$⊂Rh$_4$Ru$_3$
chemical formula	$C_{62}H_{65}Co_4CsN_{12}Ru_3$	$C_{82}H_{105}CsN_{12}Rh_4Ru_3$	$C_{82}H_{109}N_{13}Rh_4Ru_3$
temp (K)	193(2)	193(2)	193(2)
crystal size (mm^3)	0.24 × 0.16 × 0.10	0.60 × 0.40 × 0.40	0.65 × 0.20 × 0.18
space group	*P*2(1)/*c*	*P*2$_1$/*n*	*Pnma*
a (Å)	15.414(7)	14.926(12)	25.987(10)
b (Å)	25.048(12)	48.475(4)	17.203(6) A
c (Å)	23.332(11)	16.093(12)	23.432(9) A
α (deg)	90	90	90
β (deg)	104.807(10)	104.076(5)	90
γ (deg)	90	90	90
V (Å^3)	8709(7)	11 293.9(15)	10 475(7)
Z	4	4	4
D_{calcd} (Mg m^{-3})	1.540	1.480	1.403
μ (Mo Kα, mm^{-1})	1.715	1.330	1.084
min and max trans'n	0.6066/0.8481	0.4688/0.6957	0.5294/0.8395
reflections meas'd/indep.	45 846/15 947	67 845/19 946	103 582/9981
data/restraints/parameters	15 947/27/955	19 946/994/991	9981/161/675
GOF	0.876	1.341	1.050
R_{int}	0.0680	0.0419	0.0485
R_1 [$I > 2\sigma$] (all data)[a]	0.0651 (0.1399)	0.1215 (0.1285)	0.0284 (0.0355)
wR_2 [$I > 2\sigma$] (all data)[b]	0.1555 (0.1882)	0.2541 (0.2569)	0.0672 (0.0698)
max peak/hole (e/Å^3)	2.806/−1.155	3.225/−2.090	0.589/−1.565

[a] $R_1 = \sum||F_o| - |F_c||/\sum|F_o|$. [b] $wR_2 = \{\sum[w(F_o^2 - F_c^2)^2]/\sum[w(F_o^2)^2]\}^{1/2}$.

After being stirred for 1 h, the solution was allowed to stand for 24 h before the solvent was removed in vacuo. The yellow solid was extracted into 150 mL of Et_2O, and this extract was filtered to remove Et_4NPF_6. Evaporation of the filtrate afforded a fine golden yellow powder. Yield: 350 mg (66%). ^{1}H NMR (THF-d_8): δ 1.628 (s, 15H), 1.652 (s, 30H), 2.004 (s, 30H), 2.008 (s, 15H), and 2.046 (s, 15H). ^{133}Cs NMR (THF): δ 92.0 (s). IR (MeCN, cm^{-1}): ν_{CN} = 2158, 2142, 2124, and 2121. ESI-MS: m/z = 2107 ([M$^+$]). Anal. Calcd for $C_{82}H_{95}CsN_{12}Rh_4Ru_3$: C, 46.78; H, 5.02; N, 7.98. Found: C, 45.75; H, 5.20; N, 7.53. Crystals of **Cs⊂Rh$_4$Ru$_3$** were obtained by cooling a saturated THF solution of **Cs⊂Rh$_4$Ru$_3$**.

NH$_4$⊂[Cp*Rh(CN)$_3$]$_4$[Cp*Ru]$_3$ (NH$_4$⊂Rh$_4$Ru$_3$). A solution of 611 mg (1.211 mmol) of [Cp*Ru(NCMe)$_3$]PF$_6$ in 50 mL of MeCN was added dropwise to a solution of 66 mg (0.404 mmol) of NH_4PF_6 and 750 mg (1.615 mmol) of Et_4N[Cp*Rh(CN)$_3$] in 325 mL of MeCN. After being stirred for 1 h, the solution was allowed to stand for 24 h before the solvent was removed in vacuo. The yellow solid was extracted into 150 mL of Et_2O, and this extract was filtered to remove Et_4NPF_6. Evaporation of the filtrate afforded a fine golden yellow powder. Yield: 610 mg (76%). IR (MeCN, cm^{-1}): ν_{CN} = 2119, 2147, 2160; ν_{NH} = 3270 (sh), 3246, and 3196. ^{1}H NMR (THF): δ 1.63 (s, 15H), 1.66 (s, 30H), 2.00 (s), 2.01 (s, 45H), 2.04 (s, 15H), and 5.40 (m, 4H). ESI-MS: m/z = 1992 ([M$^+$]). Anal. Calcd for $C_{82}H_{99}N_{13}Rh_4Ru_3$: C, 49.45; H, 5.52; N, 9.14. Found: C, 49.53; H, 5.43; N, 8.88. Crystals of **NH$_4$⊂Rh$_4$Ru$_3$** were obtained by layering a THF solution of **NH$_4$⊂Rh$_4$Ru$_3$** with MeCN and hexane.

Cage Formation Monitored by ESI-MS. A solution of 49 mg (0.097 mmol) of [Cp*Ru(NCMe)$_3$]PF$_6$ in 10 mL of MeCN was added dropwise to a solution of 9 mg (0.032 mmol) of CsOTf and 60 mg (0.129 mmol) of Et_4N[Cp*Rh(CN)$_3$] in 10 mL of MeCN. The reaction was monitored by negative and positive mode ESI-MS at 1, 4, 11, and 24 h. ESI-MS samples were diluted with MeCN to give 10^{-11} mol/μL concentrations. Experiments were run in duplicate with a MS/MS experiment following each interval. In these experiments, the cone voltage was varied between 25 and 35 V with no effect on the ion abundances.

^{133}Cs NMR Measurements. Measurements were conducted at 66 MHz on a Varian Unity INOVA 600 spectrometer with the following settings: delay time of 2 s, pulse width of 15 μs, and acquisition times were typically 2.0 s. Samples were approximately 5 mM (MeCN or THF solvent) in 5 mm tubes. Chemical shifts were referenced to a 1 M CsOTf solution of MeCN at δ34.362.

The ^{133}Cs MAS NMR measurements were conducted at 66 MHz on a Varian Unity INOVA 750 spectrometer with the following settings: delay time of 1 s, pulse width of 8.3 μs, and acquisition times were typically 0.5 s.

Conversion of NH$_4$⊂Rh$_4$Ru$_3$ into Cs⊂Rh$_4$Ru$_3$. A solution of 7 mg (0.025 mmol) of CsOTf in 3 mL of CD_3CN was added to a solution of 50 mg (0.025 mmol) of **NH$_4$⊂Rh$_4$Ru$_3$** in 3 mL of CD_3CN, which was immediately (25 min) monitored by ^{133}Cs NMR, showing a single signal at δ 88. A similar experiment was performed by ^{1}H NMR.

Competition Experiment of BC6B versus NH$_4$⊂[Cp*Rh(CN)$_3$]$_4$-[Cp*Ru]$_3$. A solution of 7 mg (0.026 mmol) of CsOTf and 24 mg (0.026 mmol) of calix[4]arene-bis(benzocrown-6) in 12 mL of CD_3CN was allowed to stand for 24 h. The solution was then monitored by ^{133}Cs NMR, which revealed one signal at −17 ppm and no free cesium at 34 ppm. A solution of 52 mg (0.026 mmol) of **NH$_4$⊂Rh$_4$Ru$_3$** in 3 mL of CD_3CN was added to the initial solution of CsOTf and calix[4]arene-bis(benzocrown-6). The solution was immediately monitored (approximately 1 h) by ^{133}Cs NMR, which revealed one signal at δ 88. A similar experiment was run in THF solvent, which yielded a similar result. The calix[4]arene-bis(benzocrown-6) ligand was obtained from ACROS.

Crystallography. Crystals were mounted on thin glass fibers using Paratone-N oil (Exxon) before being transferred to a Siemens Platform/CCD automated diffractometer for data collection. Data processing was performed with SAINT PLUS version 6.22. Structures were solved using direct methods and refined using full matrix least squares on F^2 using the program Bruker SHELXTL version 6.10. Hydrogen atoms were fixed in idealized positions with thermal parameters 1.5× those of the attached carbon atoms. The data were corrected for absorption on the basis of Ψ-scans. Specific details for each crystal are given in Table 2. Full crystallographic details have been deposited with the Cambridge Crystallographic Data Center.

Acknowledgment. This research was supported by the Department of Energy. We thank Scott Wilson and Teresa Prussak-Wieckowska for assistance with the X-ray crystallography.

Supporting Information Available: Crystallographic data (CIF format) including experimental details and complete tables of bond distances and angles, atomic coordinates, and anisotropic displacement parameters (PDF). This material is available free of charge via the Internet at http://pubs.acs.org.

JA035253H